universe

MDPI

Article

Update on WASP-19

Judith Korth [1,*] and Hannu Parviainen [2,3]

[1] Lund Observatory, Division of Astrophysics, Department of Physics, Lund University, Box 43, 22100 Lund, Sweden
[2] Departamento de Astrofísica, Universidad de La Laguna (ULL), E-38206 La Laguna, Tenerife, Spain
[3] Instituto de Astrofísica de Canarias (IAC), E-38200 La Laguna, Tenerife, Spain
* Correspondence: judith.korth@fysik.lu.se

Abstract: Tidal interaction between a star and a close-in massive exoplanet causes the planetary orbit to shrink and eventually leads to tidal disruption. Understanding orbital decay in exoplanetary systems is crucial for advancing our knowledge of planetary formation and evolution. Moreover, it sheds light on the broader question of the long-term stability of planetary orbits and the intricate interplay of gravitational forces within stellar systems. Analyzing Transiting Exoplanet Survey Satellite (*TESS*) data for the ultra-short period gas giant WASP-19, we aim to measure orbital period variations and constrain the stellar tidal quality parameter. For this, we fitted the *TESS* observations together with two WASP-19 transits observed using the Las Cumbres Observatory Global Telescope (LCOGT) and searched for orbital decay in combination with previously published transit times. As a result, we find a deviation from the constant orbital period at the 7σ level. The orbital period changes at a rate of $\dot{P} = -3.7 \pm 0.5$ ms year^{-1}, which translates into a tidal quality factor of $Q'_\star = (7 \pm 1) \times 10^5$. We additionally modeled WASP-19 b's phase curve using the new *TESS* photometry and obtained updated values for the planet's eclipse depth, dayside temperature, and geometric albedo. We estimate an eclipse depth of 520 ± 60 ppm, which is slightly higher than previous estimates and corresponds to a dayside brightness temperature of 2400 ± 60 K and geometric albedo of 0.20 ± 0.04.

Keywords: planets and satellites: individual: WASP-19 b; exoplanets; transit timing variations; phase curves

Citation: Korth, J.; Parviainen, H. Update on WASP-19. *Universe* **2024**, *10*, 12. https://doi.org/10.3390/universe10010012

Academic Editors: Tamás Borkovits and Szilard Csizmadia

Received: 11 December 2023
Revised: 24 December 2023
Accepted: 25 December 2023
Published: 27 December 2023

1. Introduction

Ultra-short period (USP) gas giants, a class of exoplanets characterized by their mass ($M_\mathrm{p} > 0.5\,M_\mathrm{J}$) and proximity to their host stars ($P < 1$ day), provide a unique opportunity to study the effect of tidal interactions on the evolution of stellar and planetary systems (e.g., [1]). The proximity to their hosts also means that their atmospheres can be studied using phase curves, even in the optical passbands (e.g., [2]). Unfortunately, only a few planets have been discovered in this regime, including TOI-2109 b [3], NGTS-10 b [4], and WASP-19 b [5], all exhibiting the shortest orbital periods ($P < 0.8$ day) detected so far. This paucity of USP hot Jupiters may be explained by tidal interactions that ultimately lead to tidal disruption of the planet [6,7].

Such close-in planets that are not in tidal equilibrium are expected to gradually spiral towards their host stars due to tidal dissipation (e.g., [8,9]). This phenomenon, known as tidal orbital decay, means that, due to tides raised by a close-in planet, the tidal bulge of the star exerts a torque on the planet. This torque transfers energy and angular momentum from the planet's orbit to the stellar spin (e.g., [10,11]). Consequently, the stellar rotational period decreases, and the orbit of the planet shrinks [12].

Orbital decay can be detected through its effect on the timing of transits due to its change in orbital period (e.g., [13,14]). This approach found evidence for orbital decay in WASP-12 b [15–20] and Kepler-1658 b [21]. Among the USP gas giant planets, WASP-19 b, with an orbital period of 0.78 days, has emerged as a prime target for the search for orbital

decay using transit timings [22–25]. Some studies predict a measurable effect on WASP-19 b's transit times after 10 years. The magnitude of the transit shift, however, varies from 11 s [1] to 70 s [14] to 257 s [23].

The analysis of WASP-19 b's transit timings and the exploration of potential orbital decay have been subjects of numerous studies, yielding conflicting outcomes [20,24,26–31]. While some studies report significant orbital period changes [24,28], others find no evidence for a shrinking orbit [20,26,27,29–31]. Stellar spot activity, as detected by several studies [26,31,32], may contribute to these inconsistencies, as highlighted by Patra et al. [24]. Given the divergent findings, continued monitoring of WASP-19 b's transit times and further investigations into potential period changes are essential.

WASP-19 b's short orbital period also makes it an excellent target for phase curve studies. The dayside of the planet can be expected to be hot enough for thermal emission to be detected in the optical *TESS* passband, and recent studies hint that the planet may have a higher albedo than what is generally expected for ultra-hot Jupiters, also leading to a strong reflected light signal [33,34].

Here, we present an analysis of the transit times of WASP-19 b using new ground-based and space-based observations to search for orbital decay and to set constraints on the tidal quality factor. Our analysis further improves upon the previous studies by using a logistic error distribution to model the observational errors instead of a normal distribution. This approach makes the estimation of the orbital decay posterior more robust against outliers arising from stellar activity and instrumental sources. We additionally present a phase curve analysis that is based on the new *TESS* photometry used in the orbital decay analysis. The previous *TESS* WASP-19 b phase curve analysis by Wong et al. [33] was based on the *TESS* Sector 9 light curve, while the analysis of Eftekhar and Adibi [34] used *TESS* Sectors 9 and 36. We improve upon these by modeling *TESS* Sectors 9, 36, 62, and 63 jointly without phase folding or pre-whitening of the photometry and by representing the stellar variability as a Gaussian Process (GP) with hyperparameters as free parameters in the posterior sampling.

2. Observation and Data Reduction

2.1. TESS Photometry

The Transiting Exoplanet Survey Satellite (*TESS*; [35]) observed 115 transits of WASP-19 b with a two-minute cadence during *TESS* Sectors 9, 39, 62, and 63. The *TESS* Presearch Data Conditioning (PDC) photometry [36–38], generated by the Science Processing Operations Center (SPOC) pipeline [39], was utilized. The photometry exhibits an average point-to-point (ptp) scatter of 3000 ppm.

2.2. LCOGT Photometry

We observed four full transits of WASP-19 b with the Sinistro cameras installed in the Las Cumbres Observatory Global Telescope ([40]; LCOGT) network 1.0 m telescopes. The first transit was observed from the South African Astronomical Observatory (SAAO) on 27 December 2022, the second from the Cerro Tololo Inter-American Observatory (CTIO) on 29 December 2022, the third from CTIO on 4 December 2023, and the fourth from SAAO on 13 December 2023. The observations were scheduled through `TESS Transit Finder`, a customized version of the `Tapir` software package [41], spanning three hours centered around the expected transit center. Sloan i' passband was used with 20 s exposure times, resulting in average ptp scatters of 2400, 1400, 2000, and 2400 ppm. The difference in the scatter can be attributed to observing conditions. The raw frames were reduced with the standard LCOGT `BANZAI` pipeline [42], and the relative photometry was computed using our own LCOGT photometry pipeline based on the MuSCAT2 photometry pipeline [43].

3. Theory and Numerical Methods

3.1. Estimation of Transit Center Times

The direct detection of orbital decay is possible through its effect on the transit times, as suggested by Ragozzine and Wolf [13] and Birkby et al. [14]. Orbital decay will cause a shift in the transit center times following Ragozzine and Wolf [13]:

$$T_{\rm mid} \simeq T_0 + NP + \frac{1}{2}N^2 P\dot{P}, \tag{1}$$

where $T_{\rm mid}$ is the transit center time, T_0 is the zero epoch, N is the transit number, P is the orbital period, and $\dot{P} = {\rm d}P/{\rm d}t$ is the change in the orbital period over time.

We searched for long-term transit variations resulting from orbital decay in WASP-19 b's transit times. For this, we simultaneously fitted *TESS* photometry with the two LCOGT transits using the Python Tool for Transit Variation (`PyTTV`) to estimate transit center times, following the approach described in Korth et al. [44]. The transits from *TESS* and LCOGT are modeled with the quadratic transit model by Mandel and Agol [45], incorporating the Taylor-series expansion from Parviainen and Korth [46] as implemented in `PyTransit` [47]. The fit uses orbital period, P, zero epoch T_0, planet radius relative to stellar radius $Rp/R_\star \equiv k$, transit center times $T_{\rm c}$, and impact parameter $b = a/R_\star \cos i$, where a is the semi-major axis, $R_\star$ is the radius of the star, and i is the orbital inclination, as free parameters. Shared parameters during the fit included quadratic limb darkening parameters q_1, q_2, as introduced in Kipping [48], and the stellar density $\rho_\star$. The LCOGT observations were carried out in the Sloan i' band that is similar enough to the *TESS* band that we do not need to care about the differences in limb darkening between the two datasets. Thus, we used one set of limb darkening coefficients shared by the *TESS* and LCOGT data. To address known stellar activity in the WASP-19 b light curve data, the baseline was modeled as a Gaussian Process (GP) with a Matérn 3/2 kernel, as implemented in `celerite` [49]. We set wide normal priors on P, T_0, and k, where the prior means correspond to the values reported in Hebb et al. [5]. Uniform priors were used for other parameters, and parameter posteriors were estimated through Markov chain Monte Carlo (MCMC) sampling as implemented in `emcee` [50].

We combined the newly estimated transit center times with those reported in Kokori et al. [28] as part of the ExoClock project [51,52] and in Petrucci et al. [27] to extend our baseline. Kokori et al. [28] already provided transit center estimates for *TESS* Sectors 9 and 36. However, as we simultaneously fit these sectors with the new Sectors 62 and 63, not covered by their dataset, along with LCOGT observations, we consequently excluded their *TESS* center times and utilized our calculated values instead. Additionally, we incorporated center times observed and published by Mancini et al. [26] and Patra et al. [24], which were not part of the ExoClock collection. A list of the transit times is reported in Table A1.

3.2. Estimation of Orbital Period Change

We estimate the change of WASP-19 b's orbital period over time, $\dot{P}$, using a basic Bayesian parameter estimation approach where we infer the posterior densities for Equation (1) parameters given our transit center data set. The unnormalized log posterior probability density is defined as:

$$\log P(\boldsymbol{\theta}|\boldsymbol{t}, \boldsymbol{\sigma}) = \log P(\boldsymbol{\theta}) + \log P(\boldsymbol{t}, \boldsymbol{\sigma}|\boldsymbol{\theta}), \tag{2}$$

where $\boldsymbol{\theta}$ is a vector containing the model parameters T_0, P, and $\dot{P}$; $\boldsymbol{t}$ is a vector containing the transit center times; $\boldsymbol{\sigma}$ is a vector containing the center time uncertainties; $\log P$ is the

log prior density; and log L is the log likelihood. We assume the transit center uncertainties are independent and follow a logistic distribution, which leads to a log likelihood:

$$\log P(\boldsymbol{t}, \boldsymbol{\sigma}|\boldsymbol{\theta}) = \sum_i \log\left(\frac{e^{-(t_\mathrm{i}-m_\mathrm{i})/s_\mathrm{i}}}{s_\mathrm{i}\left(1+e^{-(t_\mathrm{i}-m_\mathrm{i})/s_\mathrm{i}}\right)}\right), \tag{3}$$

where $s_\mathrm{i} = \sigma_\mathrm{i}\sqrt{3}/\pi$, and m_i are the transit mid-center time model values (Equation (1)). We use a logistic error distribution instead of a normal one because its heavier tails make it more robust to individual outliers and because its scale parameter, s, is directly related to the distribution's variance.

We set weakly informative normal priors on the zero epoch, period, and period change. For zero epoch, we use $N(\mu = 2457518.131796, \sigma = 0.01)$, where the value corresponds to the measured transit center time nearest the center of the time span covered by the observations. For period, we use $N(\mu = 0.7888399, \sigma = 0.001)$ based on Hebb et al. [5]. Finally, for $\dot{P}$, we use a wide zero-centered prior, $N(\mu = 0, \sigma = 10^{-8})$. The role of the priors is mainly to help the optimizer and the MCMC sampler, and we checked that the priors did not significantly constrain the posteriors after the MCMC sampling phase.

We inferred the posterior densities for Equation (1) parameters by first finding the global posterior mode using a differential evolution global optimizer implemented in `PyTransit`. Next, we obtained a sample from the posterior using the `emcee` MCMC sampler started with a parameter vector population created by the differential evolution optimizer. We used a parameter vector population size of 50, ran the `emcee` sampler over 50,000 iterations, and created the final posterior from the last 10,000 iterations using a thinning factor of 50. This led to a final sample size of 10,000. Considering the simplicity of the model, the optimization and MCMC sampling take less than a minute of computing time on a normal laptop computer.

3.3. Estimation of Tidal Quality Factor

Orbital decay translates into a constant change in the orbital period under the assumption of zero stellar obliquity, negligible tidal dissipation, circularized orbits, and synchronized stellar spin within the simplified constant phase lag model [16,53], as:

$$\dot{P} = -\frac{27\pi}{2Q'_\star}\left(\frac{M_\mathrm{p}}{M_\star}\right)\left(\frac{R_\star}{a}\right)^5, \tag{4}$$

where $Q'_\star$ is the tidal quality factor defined as $Q'_\star = 3Q_\star/2k_{2,\star}$ in [54], with the dissipation factor $Q_\star = 1/\Delta t$ assuming a contact time lag model and a stellar Love number $k_{2,\star}$, M_p is the planet mass, $M_\star$ is the stellar mass, and $R_\star/a$ is the stellar radius relative to the semi-major axis. Solving for $Q'_\star$, we obtain:

$$Q'_\star = \frac{-27\pi}{2}\left(\frac{M_\mathrm{p}}{M_\star}\right)\left(\frac{R_\star}{a}\right)^5\frac{1}{\dot{P}}, \tag{5}$$

where the planet–star mass ratio, $M_\mathrm{p}/M_\star$, is obtained from RV mass measurements, the scaled semi-major axis, $a/R_\star$, from transit light curve modeling, and the change of orbital period in time, $\dot{P}$, from the transit center time modeling described earlier in Section 3.1.

3.4. Phase Curve Analysis

The phase curve analysis closely follows the analyses detailed in [2,55]. We change the modeling approach slightly by assuming that the dayside brightness temperature equals its equilibrium temperature: [56]

$$T_\mathrm{Eq} = T_\star a_\mathrm{s}^{-1/2}[f(1-A_\mathrm{B})]^{1/4}, \tag{6}$$

where $T_\star$ is the stellar effective temperature, a_s is the scaled semi-major axis ($a_s = a/R_\star$), f is the heat redistribution factor, and A_B is the Bond albedo. We fix the effective stellar temperature to 5500 K [5] and set a normal prior on the heat redistribution factor, $N(0.66, 0.02)$, to focus on the solutions with low heat redistribution, since previous studies suggest that WASP-19 b's nightside is cool [33,34].

4. Results

The results from the transit center time analysis are shown in Figure 1. We find a deviation from the constant period at a 7σ level. The orbital period changes at a rate of $\dot{P} = -3.7 \pm 0.5\,\mathrm{ms\,year^{-1}}$, which translates into a tidal quality factor of $Q'_\star = (7 \pm 1) \times 10^5$, assuming a planet–star mass ratio of 0.00116 ± 0.00005 taken from [26] and a scaled semi-major axis of 3.57 ± 0.03 from our transit light curve modeling (Table 1). The posterior distributions for both quantities are shown in Figure 2.

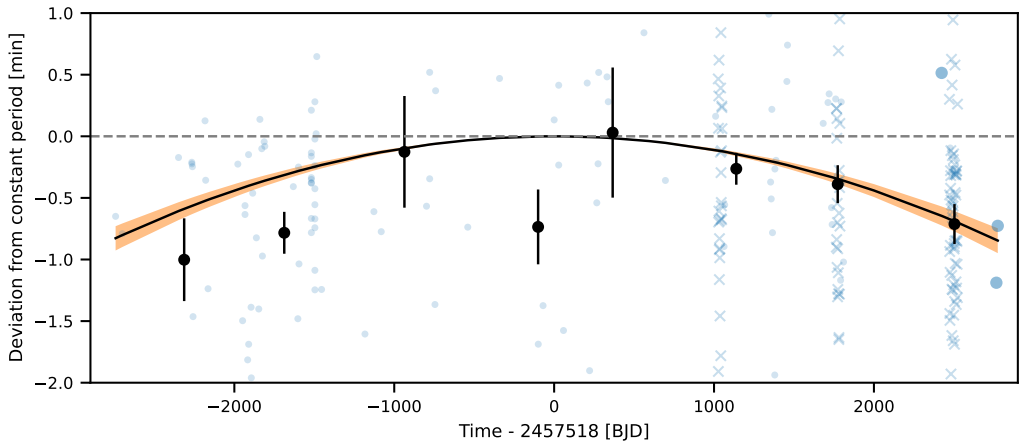

Figure 1. Posterior TTV model with blue points, crosses, and dots showing the individual transit center time values for archival data, fitted *TESS* observations, and fitted LCOGT observations, respectively. Black dots with error bars show the transit center times binned to two years, the solid black line shows the median posterior TTV model, and the orange shading shows the 68% central posterior limits.

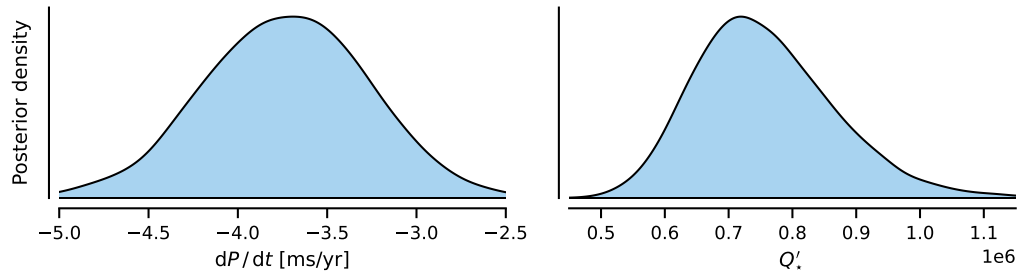

Figure 2. Posterior densities for $\dot{P}$ and $Q'_\star$. The derivation of these posteriors is detailed in Sections 3.2 and 3.3.

We show our final phase curve model in Figure 3. We obtain a *TESS* passband eclipse depth, D_e, of 520 ± 60 ppm, corresponding to a geometric albedo, A_g, of 0.20 ± 0.04 and equilibrium temperature of 2400 ± 60 K. We do not detect any offsets in the hotspot location and cannot claim that the *TESS* photometry would be able to constrain the planet's nightside brightness temperature. We also obtain improved stellar, orbital, and planetary parameters from the analysis and list them in Table 1.

Table 1. Stellar and planetary parameters for WASP-19 system from the literature and our analyses.

Literature stellar and planetary parameters				
$M_\star$ [$M_\odot$]	$R_\star$ [$R_\odot$]	$T_{\rm eff}$ [K]	$\log g$	[Fe/H]
0.935 ± 0.042 [a]	1.018 ± 0.015 [a]	5500 ± 100 [b]	4.3932 ± 0.0067 [a]	0.02 ± 0.09 [b]
$P_{\rm rot}$ [days]	Age [Gyr]	e	$M_{\rm p}$ [$M_{\rm Jup}$]	
11.76 ± 0.09 [c]	$11.5^{+2.8}_{-2.7}$ [c]	< 0.02 [d]	1.139 ± 0.036 [a]	
Fitted parameters				
P [days]	T_0 [days]	$R_{\rm p}/R_\star$	$a/R_\star$	b
$0.78883894 \pm 6 \times 10^{-8}$	$2,455,168.9690 \pm 0.0003$	0.146 ± 0.001	3.57 ± 0.03	0.65 ± 0.01
$\rho_\star$ [g cm^{-3}]	$A_{\rm g}$	$D_{\rm e}$ [ppm]	$\dot{P}$ [ms year^{-1}]	$Q'_\star$
1.39 ± 0.03	0.20 ± 0.04	520 ± 60	-3.7 ± 0.5	$(7 \pm 1) \times 10^5$

[a] Mancini et al. [26], [b] Hebb et al. [5], [c] Tregloan-Reed et al. [31], [d] Hellier et al. [57].

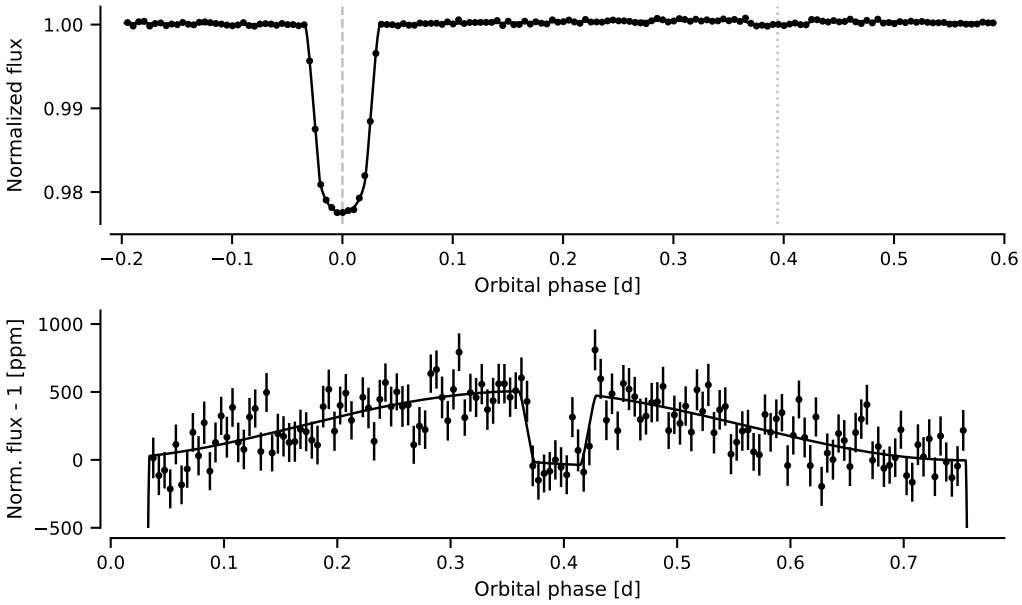

Figure 3. Phase curve of WASP-19 b. The upper panel shows the full phase curve, including the transit, and the lower plot shows a zoomed view centered around the secondary eclipse. We have removed the median Gaussian Process baseline model from the photometry and phase-folded and binned it for visualization.

5. Discussion and Conclusions

We find a significant orbital decay of $\dot{P} = -(1.2 \pm 0.1) \times 10^{-10}$ for WASP-19 b using the *TESS*, LCOGT, and archival transit times, which agrees within the uncertainties with the results from Patra et al. [24] of $\dot{P} = -(2.06 \pm 0.42) \times 10^{-10}$ and Kokori et al. [28] of $\dot{P} = (-0.87 \pm 0.13) \times 10^{-10}$. In contrast, Rosário et al. [29] found no significant evidence for orbital decay, with a rate of $\dot{P} = (-0.35 \pm 0.22) \times 10^{-10}$. Petrucci et al. [27] also failed to detect a statistically significant estimate for $\dot{P}$, but our estimate of $\dot{P} = -3.7 \pm 0.5$ ms year^{-1} agrees with their upper limit of $\dot{P} = -2.3$ ms year^{-1}. Ivshina and Winn [30] found a variation near the 3σ limit of $\dot{P} = -3.54 \pm 1.18$ ms year^{-1} that agrees well with our values for the orbital decay of WASP-19 b. Finally, Yeh et al. [20] observed variations in transit times but did not attribute them to orbital decay.

During the writing of this paper, another study was published that searched for long-term orbit period variations of hot Jupiters using the latest *TESS* Sectors 62 and 63, including WASP-19 b [58]. They found different values for $\dot{P}$ depending on the inclusion of two transit center times published by [27,32] and reported the detection as marginal. Our approach is less sensitive to individual outliers due to our use of a robust error distribution. Even then, testing how our $\dot{P}$ estimate changes by removing the same transit center time estimates as

removed by Wang et al. [58] leads to qualitatively similar behavior as by Wang et al. [58]: our $\dot{P}$ value changes by $\approx 1\sigma$ after the removal of the point at 2,457,796.59224 but agrees closely again with the original $\dot{P}$ estimate after the removal of the point at 2,457,448.71292. This sensitivity can be explained by the nature of the two estimates: the first is from transmission spectroscopy observations observed with the Hubble Space Telescope (HST) by Espinoza et al. [32], and the second is from similar observations carried out with the Very Large Telescope (VLT) by Sedaghati et al. [59]. Both transit center time estimates have six times smaller uncertainties (≈6 s) than the median uncertainty in the final dataset (≈40 s), so the two points can be expected to have an impact on the final $\dot{P}$ result.

As reported in previous studies [24,26,31,32], the differences in $\dot{P}$ might be attributed to stellar activity. One of our LCOGT observations shows a significant 6 ± 1 min deviation from the transit center time expected based on our best-fit linear ephemeris (see Figure 4, LCOGT observation 29.12.2022). The light curve shows slightly higher amplitude baseline variations than the other LCOGT-observed light curves, but the amplitude of the center time discrepancy is still curious. The Gaussian Process baseline variability should be reflected in the transit center time posteriors (that is, the transit center posterior should still agree with the linear ephemeris within uncertainties), and our analysis does not support the conclusion that the discrepancy would be due to photometric variability.

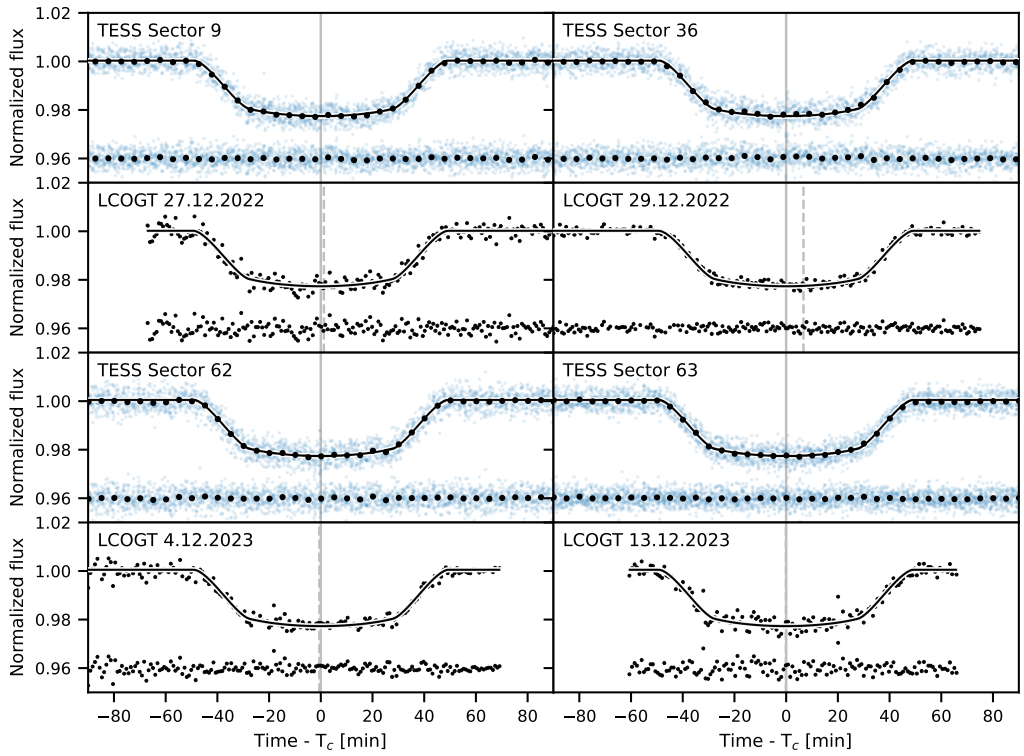

Figure 4. The newly-fitted WASP-19 b transits observed with *TESS* and the LCOGT 1 m telescopes. We center the *TESS* transits for each Sector around their fitted transit center times and bin the centered photometry over five minutes for visualization, but show the LCOGT transits individually without binning. The blue dots show the *TESS* photometry with the GP baseline removed, and black points show the binned *TESS* photometry and the LCOGT photometry with the GP baseline removed; the black line shows the transit model; the dashed gray vertical line shows the expected transit center based on best-fit linear ephemeris; and the solid black vertical line marks $T - T_c = 0$.

A parameter to quantify orbital decay is the tidal quality factor $Q'_\star$, as introduced by Goldreich and Soter [53]. This factor characterizes the efficiency of energy dissipation during tidal interactions. A higher $Q'_\star$ value indicates that the star is less efficient at dissipating tidal energy, resulting in weaker tidal forces and slower changes in the system

over time. Conversely, a lower $Q'_\star$ value suggests more efficient dissipation, leading to stronger tidal forces and faster evolution of the system. The exact value for $Q'_\star$ for a particular star is uncertain, and there is no way to measure it directly except via orbital decay (e.g., [14]). Theoretical modeling of $Q'_\star$ is also challenging because the strength of tidal decay depends on various factors, encompassing stellar properties like age, mass, interior structure, and rotation rate, as well as planet properties like orbital period and mass. Additional influences involve the conversion of tidal energy to heat, as well as the mass of the stellar convective fluid envelope (e.g., [1,23,60]).

Considering our $\dot{P}$ value as a secure detection of orbital decay, we derived a tidal quality factor of $Q'_\star = (7 \pm 1) \times 10^5$. This value agrees with the $Q'_\star$ range of $10^5 < Q'_\star < 10^6$ for gas giants in our solar system [53,61]. Several authors have calculated theoretical $Q'_\star$ values of magnitude 10^6 for WASP-19 [62–64]. However, our $Q'_\star$ value agrees more with the calculations from Essick and Weinberg [23], who derived a range of $Q'_\star$ values from 10^5 to 10^6. Additionally, Weinberg et al. [25] estimated $Q'_\star < 10^6$ for systems similar to WASP-19 b with $M_\star < 1.1 M_\odot$ and $P < 1$ day, in agreement with our $Q'_\star$.

A decreasing orbital period can also be caused by mechanisms other than orbital decay. One of them is the Rømer effect, which is a light–time effect (LTE) induced by a wide-orbit companion [65]. Whether the observed period change is caused by the Rømer effect instead of orbital decay can only be solved through radial velocity measurements over a long time span. Another mechanism that can cause long-term TTVs is produced through apsidal precession of eccentric orbits [13]. Whether WASP-19 b's eccentricity is large enough to produce apsidal precession can be solved by future eclipse center time observations. While orbital decay leads to decreasing periods of the transit and eclipse times, apsidal precession leads to an anti-correlated period trend between transit and eclipse center times. In addition, Watson and Marsh [66] calculated that the Applegate effect can have a measurable influence on USP gas giants depending on the stellar activity cycle. Whether this is the case for WASP-19 b can be tested by extending the observing time span to several stellar activity cycles.

Our secondary eclipse depth of 520 ± 60 ppm agrees with the value of 494^{+59}_{-48} ppm by Eftekhar and Adibi [34] and the value of 470^{+130}_{-110} ppm by Wong et al. [33]. Our uncertainties are similar to those by Eftekhar and Adibi [34], even when their analysis was based on only two *TESS* Sectors, but this can be explained by our differences in baseline modeling and data pre-whitening. Eftekhar and Adibi [34] detrend the *TESS* photometry before the phase curve analysis, which can easily lead to underestimated uncertainties, since the uncertainties in the stellar variability and systematics are not included in the analysis robustly. Our approach using GPs to model the baseline flux should be more reliable and also lead to more reliable uncertainties.

We repeated the phase curve analysis using individual *TESS* Sectors to test for possible time variations in any of the model parameters. The analyses did not show any variability, and it appears that the parameters are stable from *TESS* Sector to Sector.

Author Contributions: Conceptualization, J.K. and H.P.; methodology, J.K. and H.P.; software, J.K. and H.P.; validation, J.K. and H.P.; formal analysis, J.K. and H.P.; investigation, J.K. and H.P.; resources, J.K. and H.P.; data curation, J.K.; writing—original draft preparation, J.K.; writing—review and editing, J.K. and H.P.; visualization, H.P.; supervision, J.K.; project administration, J.K.; funding acquisition, J.K. and H.P. All authors have read and agreed to the published version of the manuscript.

Funding: This research was funded by the Swedish National Space Agency (SNSA; DNR 2020-00104), the Swedish Research Council (VR: Etableringsbidrag 2017-04945), and by the Spanish Ministry of Science and Innovation with the Ramon y Cajal fellowship number RYC2021-031798-I.

Data Availability Statement: The *TESS* data presented in this study are openly available at MAST. Our LCOGT observations can be found in the GitHub repository connected to this paper.

Acknowledgments: This paper includes data collected by the *TESS* mission, obtained from the MAST data archive at the Space Telescope Science Institute (STScI). Funding for the *TESS* mission is provided by NASA's Science Mission Directorate. STScI is operated by the Association of Universities for Research in Astronomy, Inc., under NASA contract NAS 5–26555. This work makes use of observations from the Las Cumbres Observatory global telescope network.

Conflicts of Interest: The authors declare no conflicts of interest.

Abbreviations

The following abbreviations are used in this manuscript:

CTIO	Cerro Tololo Inter-American Observatory
GP	Gaussian Process
LCOGT	Las Cumbres Observatory Global Telescope
MCMC	Markov chain Monte Carlo
PDC	Presearch Data Conditioning
ptp	point-to-point
PyTTV	Python Tool for Transit Variation
SAAO	South African Astronomical Observatory
SPOC	Science Processing Operations Center
TESS	Transiting Exoplanet Survey Satellite
USP	ultra-short period

Appendix A

Table A1. Transit center times and their uncertainties with epochs calculated from reference time 2,457,518.131796 days and an orbital period of 0.78884 days.

Epoch	T_{mid} [BJD$_{\mathrm{TBD}}$]	σT_{mid} [BJD$_{\mathrm{TBD}}$]	Reference
−3477	2,454,775.33800	0.00020	[28]
−3424	2,454,817.14637	0.00021	[28]
−2978	2,455,168.96900	0.00060	[28]
−2873	2,455,251.79707	0.00014	[28]
−2872	2,455,252.58590	0.00010	[28]
−2868	2,455,255.74124	0.00012	[28]
−2863	2,455,259.68459	0.00036	[27]
−2845	2,455,273.88253	0.00072	[27]
−2768	2,455,334.62540	0.00021	[28]
−2763	2,455,338.56926	0.00023	[28]
−2744	2,455,353.55659	0.00024	[28]
−2725	2,455,368.54285	0.00212	[28]
−2508	2,455,539.72330	0.00030	[28]
−2470	2,455,569.69830	0.00036	[28]
−2456	2,455,580.74155	0.00057	[27]
−2451	2,455,584.68684	0.00019	[27]
−2451	2,455,584.68689	0.00024	[27]
−2439	2,455,594.15188	0.00168	[28]
−2430	2,455,601.25164	0.00071	[28]
−2428	2,455,602.83141	0.00046	[28]
−2425	2,455,605.19414	0.00180	[26]
−2423	2,455,606.77467	0.00022	[28]
−2422	2,455,607.56244	0.00033	[28]
−2403	2,455,622.55059	0.00026	[28]
−2401	2,455,624.12787	0.00142	[28]
−2390	2,455,632.80614	0.00025	[28]
−2361	2,455,655.68222	0.00045	[28]
−2342	2,455,670.66976	0.00064	[28]
−2333	2,455,677.77038	0.00195	[28]
−2319	2,455,688.81201	0.00333	[26]
−2318	2,455,689.60280	0.00030	[28]
−2314	2,455,692.75674	0.00255	[26]
−2313	2,455,693.54639	0.00013	[28]
−2300	2,455,703.79933	0.00411	[26]
−2299	2,455,704.59078	0.00034	[28]
−2294	2,455,708.53495	0.00015	[28]

Table A1. *Cont.*

Epoch	T_{mid} [$\mathrm{BJD_{TBD}}$]	σT_{mid} [$\mathrm{BJD_{TBD}}$]	Reference
−2068	2,455,886.81234	0.00208	[26]
−2056	2,455,896.27611	0.00210	[26]
−2032	2,455,915.20980	0.00065	[28]
−2027	2,455,919.15485	0.00103	[28]
−2023	2,455,922.30966	0.00555	[26]
−1925	2,455,999.61634	0.00029	[27]
−1925	2,455,999.61649	0.00020	[27]
−1925	2,455,999.61636	0.00016	[27]
−1925	2,455,999.61606	0.00019	[27]
−1925	2,455,999.61614	0.00030	[27]
−1925	2,455,999.61634	0.00020	[27]
−1925	2,455,999.61637	0.00013	[27]
−1925	2,455,999.61651	0.00022	[27]
−1925	2,455,999.61675	0.00033	[27]
−1897	2,456,021.70358	0.00016	[27]
−1897	2,456,021.70334	0.00017	[27]
−1897	2,456,021.70363	0.00011	[27]
−1897	2,456,021.70408	0.00012	[27]
−1897	2,456,021.70380	0.00013	[27]
−1897	2,456,021.70323	0.00017	[27]
−1897	2,456,021.70393	0.00012	[27]
−1897	2,456,021.70371	0.00014	[27]
−1897	2,456,021.70429	0.00048	[27]
−1887	2,456,029.59250	0.00035	[28]
−1882	2,456,033.53713	0.00074	[27]
−1882	2,456,033.53800	0.00040	[27]
−1882	2,456,033.53837	0.00029	[27]
−1844	2,456,063.51170	0.00030	[28]
−1513	2,456,324.62053	0.00061	[27]
−1500	2,456,334.87207	0.00052	[27]
−1429	2,456,390.88033	0.00053	[27]
−1371	2,456,436.63288	0.00065	[27]
−1012	2,456,719.82623	0.00055	[27]
−987	2,456,739.54736	0.00030	[27]
−987	2,456,739.54796	0.00005	[28]
−945	2,456,772.67789	0.00052	[24]
−940	2,456,776.62329	0.00007	[28]
−685	2,456,977.77647	0.00010	[27]
−433	2,457,176.56474	0.00009	[28]
−126	2,457,418.73682	0.00023	[27]
−88	2,457,448.71292	0.00008	[27]
0	2,457,518.13180	0.00040	[27]
36	2,457,546.53020	0.00038	[24]
36	2,457,546.52975	0.00028	[27]
41	2,457,550.47270	0.00040	[27]
74	2,457,576.50470	0.00070	[27]
262	2,457,724.80783	0.0008	[27]
281	2,457,739.79415	0.00050	[27]
329	2,457,777.65743	0.00100	[27]
338	2,457,784.75892	0.00020	[27]
348	2,457,792.64753	0.00080	[27]
353	2,457,796.59224	0.00006	[28]
419	2,457,848.65559	0.00007	[28]
429	2,457,856.54384	0.00011	[28]
712	2,458,079.78567	0.00020	[27]
750	2,458,109.76384	0.00200	[27]
882	2,458,213.88747	0.00024	[27]
1280	2,458,527.84576	0.00050	[27]
1301	2,458,544.41159	0.00049	This work
1302	2,458,545.19878	0.00046	This work
1303	2,458,545.98899	0.00042	This work
1304	2,458,546.77730	0.00044	This work
1305	2,458,547.56685	0.00044	This work
1306	2,458,548.35504	0.00042	This work
1307	2,458,549.14473	0.00047	This work
1307	2,458,549.14510	0.00050	[28]
1308	2,458,549.93162	0.00050	This work

Table A1. *Cont.*

Epoch	T_{mid} [BJD$_{\mathrm{TBD}}$]	σT_{mid} [BJD$_{\mathrm{TBD}}$]	Reference
1309	2,458,550.72134	0.00053	This work
1310	2,458,551.51001	0.00046	This work
1311	2,458,552.29908	0.00048	This work
1312	2,458,553.08802	0.00050	This work
1313	2,458,553.87665	0.00045	This work
1314	2,458,554.66554	0.00049	This work
1315	2,458,555.45400	0.00046	This work
1318	2,458,557.82144	0.00048	This work
1319	2,458,558.64753	0.04132	This work
1320	2,458,559.39948	0.00048	This work
1321	2,458,560.18681	0.00044	This work
1322	2,458,560.97747	0.00047	This work
1323	2,458,561.76552	0.00046	This work
1324	2,458,562.55410	0.00047	This work
1325	2,458,563.34303	0.00047	This work
1326	2,458,564.13185	0.00044	This work
1327	2,458,564.92100	0.00044	This work
1328	2,458,565.70945	0.00049	This work
1329	2,458,566.49893	0.00045	This work
1330	2,458,567.28776	0.00046	This work
1331	2,458,568.07648	0.00047	This work
1347	2,458,580.69724	0.00040	[24]
1352	2,458,584.64167	0.00030	[27]
1702	2,458,860.73640	0.00050	[28]
1716	2,458,871.77920	0.00070	[28]
1721	2,458,875.72330	0.00040	[28]
1726	2,458,879.66800	0.00040	[28]
1731	2,458,883.61150	0.00060	[28]
1740	2,458,890.71260	0.00040	[28]
1749	2,458,897.80980	0.00060	[28]
1750	2,458,898.59980	0.00060	[28]
1754	2,458,901.75620	0.00040	[28]
1759	2,458,905.69940	0.00030	[28]
1802	2,458,939.62040	0.00040	[28]
1845	2,458,973.54000	0.00040	[28]
1850	2,458,977.48440	0.00040	[28]
2133	2,459,200.72540	0.00030	[28]
2142	2,459,207.82650	0.00040	[28]
2171	2,459,230.70140	0.00030	[28]
2180	2,459,237.80100	0.00040	[28]
2199	2,459,252.78830	0.00040	[28]
2204	2,459,256.73240	0.00050	[28]
2232	2,459,278.82060	0.00050	[28]
2237	2,459,282.76396	0.00041	This work
2238	2,459,283.55358	0.00051	This work
2239	2,459,284.34242	0.00056	This work
2240	2,459,285.13052	0.00050	This work
2241	2,459,285.91993	0.00047	This work
2242	2,459,286.70888	0.00048	This work
2243	2,459,287.49688	0.00050	This work
2244	2,459,288.28608	0.00045	This work
2245	2,459,289.07504	0.00043	This work
2246	2,459,289.86365	0.00048	This work
2247	2,459,290.65207	0.00048	This work
2248	2,459,291.44118	0.00051	This work
2249	2,459,292.22979	0.00048	This work
2253	2,459,295.38524	0.00052	This work
2254	2,459,296.17533	0.00049	This work
2255	2,459,296.96280	0.00048	This work
2256	2,459,297.75092	0.00051	This work
2257	2,459,298.54022	0.00050	This work
2258	2,459,299.32907	0.00047	This work
2259	2,459,300.11861	0.00054	This work
2260	2,459,300.90769	0.00045	This work
2261	2,459,301.69647	0.00048	This work
2262	2,459,302.48467	0.00049	This work
2263	2,459,303.27411	0.00049	This work

Table A1. *Cont.*

Epoch	T_{mid} [BJD_{TBD}]	σT_{mid} [BJD_{TBD}]	Reference
2264	2,459,304.06390	0.00049	This work
2265	2,459,304.85215	0.00045	This work
2266	2,459,305.64041	0.00049	This work
2271	2,459,309.58430	0.00040	[28]
2276	2,459,313.52950	0.00040	[28]
2294	2,459,327.72770	0.00090	[28]
2535	2,459,517.84020	0.00040	[28]
3072	2,459,941.44552	0.00030	This work (LCOGT)
3075	2,459,943.81605	0.00035	This work (LCOGT)
3133	2,459,989.55985	0.10613	This work
3134	2,459,990.35339	0.00049	This work
3135	2,459,991.14169	0.00044	This work
3136	2,459,991.93021	0.00053	This work
3137	2,459,992.71870	0.00047	This work
3138	2,459,993.50750	0.00043	This work
3139	2,459,994.29661	0.00053	This work
3140	2,459,995.08615	0.00090	This work
3141	2,459,995.87444	0.00049	This work
3142	2,459,996.66370	0.00045	This work
3143	2,459,997.45244	0.00051	This work
3144	2,459,998.24135	0.00046	This work
3145	2,459,999.03033	0.00050	This work
3146	2,459,999.81791	0.00041	This work
3147	2,460,000.60773	0.00045	This work
3150	2,460,002.97504	0.00046	This work
3151	2,460,003.76306	0.00047	This work
3152	2,460,004.55150	0.00047	This work
3153	2,460,005.34000	0.00049	This work
3154	2,460,006.12910	0.00046	This work
3155	2,460,006.91909	0.00048	This work
3156	2,460,007.66404	0.03918	This work
3157	2,460,008.49637	0.00051	This work
3158	2,460,009.28486	0.00049	This work
3159	2,460,010.07379	0.00047	This work
3160	2,460,010.86213	0.00044	This work
3161	2,460,011.65141	0.00046	This work
3162	2,460,012.44133	0.00049	This work
3163	2,460,013.22912	0.00046	This work
3164	2,460,014.01720	0.00043	This work
3165	2,460,014.80706	0.00045	This work
3166	2,460,015.59584	0.00049	This work
3167	2,460,016.38477	0.00049	This work
3168	2,460,017.17270	0.00043	This work
3169	2,460,017.96171	0.00049	This work
3170	2,460,018.75117	0.00051	This work
3171	2,460,019.53959	0.00050	This work
3172	2,460,020.32846	0.00047	This work
3173	2,460,021.11728	0.00054	This work
3174	2,460,021.90557	0.00050	This work
3175	2,460,022.69465	0.00046	This work
3176	2,460,023.48426	0.00046	This work
3177	2,460,024.27267	0.00049	This work
3178	2,460,025.06250	0.00051	This work
3179	2,460,025.85062	0.00049	This work
3180	2,460,026.63906	0.00048	This work
3181	2,460,027.49901	0.03815	This work
3182	2,460,028.21724	0.00045	This work
3183	2,460,029.00464	0.00044	This work
3184	2,460,029.79492	0.00046	This work
3185	2,460,030.58364	0.00045	This work
3186	2,460,031.37199	0.00048	This work
3187	2,460,032.16143	0.00047	This work
3188	2,460,032.94954	0.00048	This work
3189	2,460,033.73913	0.00046	This work
3190	2,460,034.52758	0.00050	This work
3191	2,460,035.31615	0.00052	This work
3192	2,460,036.10565	0.00050	This work

Table A1. *Cont.*

Epoch	T_{mid} [BJD$_{\mathrm{TBD}}$]	σT_{mid} [BJD$_{\mathrm{TBD}}$]	Reference
3193	2,460,036.89307	0.00051	This work
3194	2,460,037.68293	0.00045	This work
3195	2,460,038.47164	0.00046	This work
3196	2,460,039.25966	0.00049	This work
3197	2,460,040.04913	0.00049	This work
3198	2,460,040.83906	0.00056	This work
3506	2,460,283.80047	0.00032	This work (LCOGT)
3517	2,460,292.47802	0.00035	This work (LCOGT)

References

1. Alvarado-Montes, J.A.; Sucerquia, M.; García-Carmona, C.; Zuluaga, J.I.; Spitler, L.; Schwab, C. The impact of tidal friction evolution on the orbital decay of ultra-short-period planets. *Mon. Not. R. Astron. Soc.* **2021**, *506*, 2247–2259. [CrossRef]
2. Parviainen, H.; Wilson, T.G.; Lendl, M.; Kitzmann, D.; Pallé, E.; Serrano, L.M.; Meier Valdes, E.; Benz, W.; Deline, A.; Ehrenreich, D.; et al. CHEOPS Finds KELT-1b Darker than Expected in Visible Light: Discrepancy between the CHEOPS and TESS Eclipse Depths. *Astron. Astrophys.* **2022**, *668*, A93. [CrossRef]
3. Wong, I.; Shporer, A.; Zhou, G.; Kitzmann, D.; Komacek, T.D.; Tan, X.; Tronsgaard, R.; Buchhave, L.A.; Vissapragada, S.; Greklek-McKeon, M.; et al. TOI-2109: An Ultrahot Gas Giant on a 16 hr Orbit. *Astron. J.* **2021**, *162*, 256. [CrossRef]
4. McCormac, J.; Gillen, E.; Jackman, J.A.G.; Brown, D.J.A.; Bayliss, D.; Wheatley, P.J.; Anderson, D.R.; Armstrong, D.J.; Bouchy, F.; Briegal, J.T.; et al. NGTS-10b: The shortest period hot Jupiter yet discovered. *Mon. Not. R. Astron. Soc.* **2020**, *493*, 126–140. [CrossRef]
5. Hebb, L.; Collier-Cameron, A.; Triaud, A.H.M.J.; Lister, T.A.; Smalley, B.; Maxted, P.F.L.; Hellier, C.; Anderson, D.R.; Pollacco, D.; Gillon, M.; et al. WASP-19b: The Shortest Period Transiting Exoplanet Yet Discovered. *Astrophys. J.* **2010**, *708*, 224–231. [CrossRef]
6. Pätzold, M.; Rauer, H. Where Are the Massive Close-in Extrasolar Planets? *Astrophys. J. Lett.* **2002**, *568*, L117–L120. [CrossRef]
7. Jackson, B.; Barnes, R.; Greenberg, R. Observational Evidence for Tidal Destruction of Exoplanets. *Astrophys. J.* **2009**, *698*, 1357–1366. [CrossRef]
8. Levrard, B.; Winisdoerffer, C.; Chabrier, G. Falling Transiting Extrasolar Giant Planets. *Astrophys. J. Lett* **2009**, *692*, L9–L13. [CrossRef]
9. Matsumura, S.; Peale, S.J.; Rasio, F.A. Tidal Evolution of Close-in Planets. *Astrophys. J.* **2010**, *725*, 1995–2016. [CrossRef]
10. Zahn, J.P. Tidal friction in close binary systems. *Astron. Astrophys.* **1977**, *57*, 383–394.
11. Hut, P. Tidal evolution in close binary systems. *Astron. Astrophys.* **1981**, *99*, 126–140.
12. Jackson, B.; Greenberg, R.; Barnes, R. Tidal Evolution of Close-in Extrasolar Planets. *Astrophys. J.* **2008**, *678*, 1396–1406. [CrossRef]
13. Ragozzine, D.; Wolf, A.S. Probing the Interiors of very Hot Jupiters Using Transit Light Curves. *Astrophys. J.* **2009**, *698*, 1778–1794. [CrossRef]
14. Birkby, J.L.; Cappetta, M.; Cruz, P.; Koppenhoefer, J.; Ivanyuk, O.; Mustill, A.J.; Hodgkin, S.T.; Pinfield, D.J.; Sipőcz, B.; Kovács, G.; et al. WTS-2 b: A hot Jupiter orbiting near its tidal destruction radius around a K dwarf. *Mon. Not. R. Astron. Soc.* **2014**, *440*, 1470–1489. [CrossRef]
15. Maciejewski, G.; Dimitrov, D.; Fernández, M.; Sota, A.; Nowak, G.; Ohlert, J.; Nikolov, G.; Bukowiecki, Ł.; Hinse, T.C.; Pallé, E.; et al. Departure from the constant-period ephemeris for the transiting exoplanet WASP-12. *Astron. Astrophys.* **2016**, *588*, L6. [CrossRef]
16. Patra, K.C.; Winn, J.N.; Holman, M.J.; Yu, L.; Deming, D.; Dai, F. The Apparently Decaying Orbit of WASP-12b. *Astron. J.* **2017**, *154*, 4. [CrossRef]
17. Yee, S.W.; Winn, J.N.; Knutson, H.A.; Patra, K.C.; Vissapragada, S.; Zhang, M.M.; Holman, M.J.; Shporer, A.; Wright, J.T. The Orbit of WASP-12b Is Decaying. *Astrophys. J. Lett.* **2020**, *888*, L5. [CrossRef]
18. Turner, J.D.; Ridden-Harper, A.; Jayawardhana, R. Decaying Orbit of the Hot Jupiter WASP-12b: Confirmation with TESS Observations. *Astron. J.* **2021**, *161*, 72. [CrossRef]
19. Wong, I.; Shporer, A.; Vissapragada, S.; Greklek-McKeon, M.; Knutson, H.A.; Winn, J.N.; Benneke, B. TESS Revisits WASP-12: Updated Orbital Decay Rate and Constraints on Atmospheric Variability. *Astron. J.* **2022**, *163*, 175. [CrossRef]
20. Yeh, L.C.; Jiang, I.G.; A-thano, N. Searching for candidates of orbital decays among transit exoplanets. *New Astron.* **2024**, *106*, 102130. [CrossRef]
21. Vissapragada, S.; Chontos, A.; Greklek-McKeon, M.; Knutson, H.A.; Dai, F.; Pérez González, J.; Grunblatt, S.; Huber, D.; Saunders, N. The Possible Tidal Demise of Kepler's First Planetary System. *Astrophys. J. Lett.* **2022**, *941*, L31. [CrossRef]
22. Valsecchi, F.; Rasio, F.A. Planets on the Edge. *Astrophys. J. Lett.* **2014**, *787*, L9. [CrossRef]
23. Essick, R.; Weinberg, N.N. Orbital Decay of Hot Jupiters Due to Nonlinear Tidal Dissipation within Solar-type Hosts. *Astrophys. J.* **2016**, *816*, 18. [CrossRef]
24. Patra, K.C.; Winn, J.N.; Holman, M.J.; Gillon, M.; Burdanov, A.; Jehin, E.; Delrez, L.; Pozuelos, F.J.; Barkaoui, K.; Benkhaldoun, Z.; et al. The Continuing Search for Evidence of Tidal Orbital Decay of Hot Jupiters. *Astron. J.* **2020**, *159*, 150. [CrossRef]

25. Weinberg, N.N.; Davachi, N.; Essick, R.; Yu, H.; Arras, P.; Belland, B. Orbital Decay of Hot Jupiters due to Weakly Nonlinear Tidal Dissipation. *arXiv* **2023**, arXiv:2305.11974. [CrossRef]
26. Mancini, L.; Ciceri, S.; Chen, G.; Tregloan-Reed, J.; Fortney, J.J.; Southworth, J.; Tan, T.G.; Burgdorf, M.; Calchi Novati, S.; Dominik, M.; et al. Physical properties, transmission and emission spectra of the WASP-19 planetary system from multi-colour photometry. *Mon. Not. R. Astron.* **2013**, *436*, 2–18. [CrossRef]
27. Petrucci, R.; Jofré, E.; Gómez Maqueo Chew, Y.; Hinse, T.C.; Mašek, M.; Tan, T.G.; Gómez, M. Discarding orbital decay in WASP-19b after one decade of transit observations. *Mon. Not. R. Astron. Soc.* **2020**, *491*, 1243–1259. [CrossRef]
28. Kokori, A.; Tsiaras, A.; Edwards, B.; Jones, A.; Pantelidou, G.; Tinetti, G.; Bewersdorff, L.; Iliadou, A.; Jongen, Y.; Lekkas, G.; et al. ExoClock Project. III. 450 New Exoplanet Ephemerides from Ground and Space Observations. *Astrophys. J. Suppl. Ser.* **2023**, *265*, 4. [CrossRef]
29. Rosário, N.M.; Barros, S.C.C.; Demangeon, O.D.S.; Santos, N.C. Measuring the orbit shrinkage rate of hot Jupiters due to tides. *Astron. Astrophys.* **2022**, *668*, A114. [CrossRef]
30. Ivshina, E.S.; Winn, J.N. TESS Transit Timing of Hundreds of Hot Jupiters. *Astrophys. J. Suppl. Ser.* **2022**, *259*, 62. [CrossRef]
31. Tregloan-Reed, J.; Southworth, J.; Tappert, C. Transits and starspots in the WASP-19 planetary system. *Mon. Not. R. Astron. Soc.* **2013**, *428*, 3671–3679. [CrossRef]
32. Espinoza, N.; Rackham, B.V.; Jordán, A.; Apai, D.; López-Morales, M.; Osip, D.J.; Grimm, S.L.; Hoeijmakers, J.; Wilson, P.A.; Bixel, A.; et al. ACCESS: A featureless optical transmission spectrum for WASP-19b from Magellan/IMACS. *Mon. Not. R. Astron. Soc.* **2019**, *482*, 2065–2087. [CrossRef]
33. Wong, I.; Benneke, B.; Shporer, A.; Fetherolf, T.; Kane, S.R.; Ricker, G.R.; Vanderspek, R.; Seager, S.; Winn, J.N.; Collins, K.A.; et al. *TESS* Phase Curve Hot Jupit. WASP-19b. *Astron. J.* **2020**, *159*, 104. [CrossRef]
34. Eftekhar, M.; Adibi, P. TESS Unveils the Full Phase Curve of WASP-19b. *Planet. Sci. J.* **2022**, *3*, 255. [CrossRef]
35. Ricker, G.R.; Winn, J.N.; Vanderspek, R.; Latham, D.W.; Bakos, G.Á.; Bean, J.L.; Berta-Thompson, Z.K.; Brown, T.M.; Buchhave, L.; Butler, N.R.; et al. Transiting Exoplanet Survey Satellite (TESS). In Proceedings of the Space Telescopes and Instrumentation 2014: Optical, Infrared, and Millimeter Wave, Montréal, QC, Canada, 22–27 June 2014; Society of Photo-Optical Instrumentation Engineers (SPIE) Conference Series; Oschmann, Jacobus M.J., Clampin, M., Fazio, G.G., MacEwen, H.A., Eds.; SPIE: St Bellingham, WA, USA, 2014; Volume 9143, p. 914320. [CrossRef]
36. Stumpe, M.C.; Smith, J.C.; Catanzarite, J.H.; Van Cleve, J.E.; Jenkins, J.M.; Twicken, J.D.; Girouard, F.R. Multiscale Systematic Error Correction via Wavelet-Based Bandsplitting in Kepler Data. *Publ. Astron. Soc. Pac.* **2014**, *126*, 100–114. [CrossRef]
37. Stumpe, M.C.; Smith, J.C.; Van Cleve, J.E.; Twicken, J.D.; Barclay, T.S.; Fanelli, M.N.; Girouard, F.R.; Jenkins, J.M.; Kolodziejczak, J.J.; McCauliff, S.D.; et al. Kepler Presearch Data Conditioning I—Architecture and Algorithms for Error Correction in Kepler Light Curves. *Publ. Astron. Soc. Pac.* **2012**, *124*, 985–999. [CrossRef]
38. Smith, J.C.; Stumpe, M.C.; Van Cleve, J.E.; Jenkins, J.M.; Barclay, T.S.; Fanelli, M.N.; Girouard, F.R.; Kolodziejczak, J.J.; McCauliff, S.D.; Morris, R.L.; et al. Kepler Presearch Data Conditioning II - A Bayesian Approach to Systematic Error Correction. *Publ. Astron. Soc. Pac.* **2012**, *124*, 1000–1014. [CrossRef]
39. Jenkins, J.M.; Twicken, J.D.; McCauliff, S.; Campbell, J.; Sanderfer, D.; Lung, D.; Mansouri-Samani, M.; Girouard, F.; Tenenbaum, P.; Klaus, T.; et al. The TESS Science Processing Operations Center. In Proceedings of the Software and Cyberinfrastructure for Astronomy IV, Edinburgh, UK, 26 June–1 July 2016; Chiozzi, G., Guzman, J.C., Eds.; SPIE: St Bellingham, WA, USA, 2016; Volume 9913, p. 99133E. [CrossRef]
40. Brown, T.M.; Baliber, N.; Bianco, F.B.; Bowman, M.; Burleson, B.; Conway, P.; Crellin, M.; Depagne, É.; De Vera, J.; Dilday, B.; et al. Las Cumbres Observatory Global Telescope Network. *Publ. Astron. Soc. Pac.* **2013**, *125*, 1031–1055. [CrossRef]
41. Jensen, E. *Tapir: A Web Interface for Transit/Eclipse Observability*; Astrophysics Source Code Library, 2013; p. ascl:1306.007.
42. McCully, C.; Volgenau, N.; Harbeck, D.R.; Lister, T.; Saunders, E.; Turner, M.L.; Siiverd, R.J.; Bowman, M. Real-Time Processing of the Imaging Data from the Network of Las Cumbres Observatory Telescopes Using BANZAI. In Proceedings of the Software and Cyberinfrastructure for Astronomy V, Austin, TX, USA, 10–15 June 2018; Guzman, J.C., Ibsen, J., Eds. SPIE: St Bellingham, WA, USA, 2018; p. 22. [CrossRef]
43. Parviainen, H.; Tingley, B.; Deeg, H.J.; Palle, E.; Alonso, R.; Montanes Rodriguez, P.; Murgas, F.; Narita, N.; Fukui, A.; Watanabe, N.; et al. Multicolour Photometry for Exoplanet Candidate Validation. *Astron. Astrophys.* **2019**, *630*, A89. [CrossRef]
44. Korth, J.; Gandolfi, D.; Šubjak, J.; Howard, S.; Ataiee, S.; Collins, K.A.; Quinn, S.N.; Mustill, A.J.; Guillot, T.; Lodieu, N.; et al. TOI-1130: A photodynamical analysis of a hot Jupiter in resonance with an inner low-mass planet. *Astron. Astrophys.* **2023**, *675*, A115. [CrossRef]
45. Mandel, K.; Agol, E. Analytic Light Curves for Planetary Transit Searches. *Astrophys. J. Lett.* **2002**, *580*, L171–L175. [CrossRef]
46. Parviainen, H.; Korth, J. Going back to basics: Accelerating exoplanet transit modelling using Taylor-series expansion of the orbital motion. *Mon. Not. R. Astron. Soc.* **2020**, *499*, 3356–3361. [CrossRef]
47. Parviainen, H. PYTRANSIT: Fast and easy exoplanet transit modelling in PYTHON. *Mon. Not. R. Astron. Soc.* **2015**, *450*, 3233–3238. [CrossRef]
48. Kipping, D.M. Efficient, uninformative sampling of limb darkening coefficients for two-parameter laws. *Mon. Not. R. Astron. Soc.* **2013**, *435*, 2152–2160. [CrossRef]
49. Foreman-Mackey, D.; Agol, E.; Ambikasaran, S.; Angus, R. Fast and Scalable Gaussian Process Modeling with Applications to Astronomical Time Series. *Astron. J.* **2017**, *154*, 220. [CrossRef]

50. Foreman-Mackey, D.; Hogg, D.W.; Lang, D.; Goodman, J. emcee: The MCMC Hammer. *Publ. Astron. Soc. Pac.* **2013**, *125*, 306. [CrossRef]
51. Kokori, A.; Tsiaras, A.; Edwards, B.; Rocchetto, M.; Tinetti, G.; Wünsche, A.; Paschalis, N.; Agnihotri, V.K.; Bachschmidt, M.; Bretton, M.; et al. ExoClock project: An open platform for monitoring the ephemerides of Ariel targets with contributions from the public. *Exp. Astron.* **2022**, *53*, 547–588. [CrossRef]
52. Kokori, A.; Tsiaras, A.; Edwards, B.; Rocchetto, M.; Tinetti, G.; Bewersdorff, L.; Jongen, Y.; Lekkas, G.; Pantelidou, G.; Poultourtzidis, E.; et al. ExoClock Project. II. A Large-scale Integrated Study with 180 Updated Exoplanet Ephemerides. *Astrophys. J. Suppl. Ser.* **2022**, *258*, 40. [CrossRef]
53. Goldreich, P.; Soter, S. Q in the Solar System. *Icarus* **1966**, *5*, 375–389. [CrossRef]
54. Dobbs-Dixon, I.; Lin, D.N.C.; Mardling, R.A. Spin-Orbit Evolution of Short-Period Planets. *Astrophys. J.* **2004**, *610*, 464–476. [CrossRef]
55. Parviainen, H. Temporal Albedo Variability in the Phase Curve of KELT-1b. *Astron. Astrophys.* **2023**, *671*, L3. [CrossRef]
56. López-Morales, M.; Seager, S. Thermal Emission from Transiting Very Hot Jupiters: Prospects for Ground-based Detection at Optical Wavelengths. *Astrophys. J. Lett.* **2007**, *667*, L191–L194. [CrossRef]
57. Hellier, C.; Anderson, D.R.; Collier-Cameron, A.; Miller, G.R.M.; Queloz, D.; Smalley, B.; Southworth, J.; Triaud, A.H.M.J. On the Orbit of the Short-period Exoplanet WASP-19b. *Astrophys. J. Lett.* **2011**, *730*, L31. [CrossRef]
58. Wang, W.; Zhang, Z.; Chen, Z.; Wang, Y.; Yu, C.; Ma, B. Long-term Orbital Period Variation of Hot Jupiters from Transiting Time Analysis using TESS Survey Data. *arXiv* **2023**, arXiv:2310.17225. [CrossRef]
59. Sedaghati, E.; Boffin, H.M.J.; MacDonald, R.J.; Gandhi, S.; Madhusudhan, N.; Gibson, N.P.; Oshagh, M.; Claret, A.; Rauer, H. Detection of titanium oxide in the atmosphere of a hot Jupiter. *Nature* **2017**, *549*, 238–241. [CrossRef] [PubMed]
60. Ogilvie, G.I. Tidal Dissipation in Stars and Giant Planets. *Annu. Rev. Astron. Astrophys.* **2014**, *52*, 171–210. [CrossRef]
61. Peale, S.J. Origin and Evolution of the Natural Satellites. *Annu. Rev. Astron. Astrophys.* **1999**, *37*, 533–602. [CrossRef]
62. Guo, S.S. The Impact of Tidal Migration of Hot Jupiters on the Rotation of Sun-like Main-sequence Stars. *Res. Astron. Astrophys.* **2023**, *23*, 095014. [CrossRef]
63. Penev, K.; Hartman, J.D.; Bakos, G.Á.; Ciceri, S.; Brahm, R.; Bayliss, D.; Bento, J.; Jordán, A.; Csubry, Z.; Bhatti, W.; et al. HATS-18b: An Extreme Short-period Massive Transiting Planet Spinning Up Its Star. *Astron. J.* **2016**, *152*, 127. [CrossRef]
64. Penev, K.; Bouma, L.G.; Winn, J.N.; Hartman, J.D. Empirical Tidal Dissipation in Exoplanet Hosts From Tidal Spin-up. *Astron. J.* **2018**, *155*, 165. [CrossRef]
65. Harre, J.V.; Smith, A.M.S. The Apparent Tidal Decay of WASP-4 b Can Be Explained by the Rømer Effect. *Universe* **2023**, *9*, 506. [CrossRef]
66. Watson, C.A.; Marsh, T.R. Orbital period variations of hot Jupiters caused by the Applegate effect. *Mon. Not. R. Astron. Soc.* **2010**, *405*, 2037–2043. [CrossRef]